43rd AIAA Aerospace Sciences Meeting and Exhibit, 10-13 January 2005, Reno, Nevada

Exact Solutions for Two-Dimensional Reactive Flow for Verification of Numerical Algorithms

Joseph M. Powers*

University of Notre Dame, Notre Dame, Indiana, 46556-5637, USA

Tariq D. Aslam†

Los Alamos National Laboratory, Los Alamos, New Mexico, 87545, USA

New exact solutions of oblique detonations are developed for the supersonic irrotational flow of an inviscid calorically perfect ideal gas which undergoes a one-step, irreversible, exothermic, zero activation energy reaction as it passes through a straight shock over a curved wedge. A full exact solution gives expressions for the velocity, pressure, density, temperature, and position as parametric functions of a variable characterizing the extent of reaction. Three limiting cases are then studied in which all variables are obtained as functions of position. The first, obtained in the asymptotic high Mach number limit, gives a simple exponential form at leading order while confining the effects of heat release to higher order. An improvement is realized in the second asymptotic limit, which better accounts for finite heat release at the expense of a more elaborate form in terms of the Lambert W function. The third, obtained for a Chapman-Jouguet condition with no additional asymptotic limits, gives all variables in terms of the Lambert W function. The solutions provide a more compact and refined description of oblique detonation; moreover, they are in harmony with long-held understanding of such flows. As the simple model employed is a rational limit of models used in the computational simulation of complex supersonic reactive flows, the solutions can serve as benchmarks for mathematical verification of general computational algorithms. An example of such a verification is given by comparing the predictions a modern shock-capturing code to those of the full exact solution. The realized spatial convergence rate is 0.779, far less than the fifth order accuracy which the chosen algorithm would exhibit for smooth flows, but consistent with the predictions of all shock-capturing codes, which never converge with greater than first order accuracy for flows with embedded discontinuities.

I. Introduction

Computational methods are increasingly being employed throughout the design process of a wide variety of aerospace applications, including those involving supersonic reactive flow with embedded shock waves. In order for the engineering community to have confidence in these predictive tools, it is necessary for the predictions to be both verified and validated (often informally called "V and V").

A. Verification and Validation

It is increasingly being recognized that the worthy goals of verification and validation are often difficult to achieve because of a variety of nuances which can arise in all stages of the modeling process.[1,2] One hurdle which too often hinders progress relates to a lack of precision in language. Here, briefly stated definitions consistent with those advocated in greater detail by Roache[3–7] are adopted: *verification* describes a process in which one ascertains whether computational predictions have fidelity with the underlying mathematical

*Associate Professor, AIAA Associate Fellow, powers@nd.edu.

†Detonation Physics Team, aslam@lanl.gov.

model, and *validation* is the independent process in which one determines how well the computational predictions are in agreement with experimental observations. While both verification and validation are necessary, it is clear that in order to determine if a mathematical model is correctly predicting the observable physics, one must *first* verify and *second* validate. The common error of neglecting to harmonize computational predictions with underlying mathematics, and instead, simply tuning the results to match those of experiments, gives rise to the strong possibility that the computational predictions depend dangerously on both the size of the discrete grid and the particular computational algorithm used to solve the underlying equations.

The issue of verification and validation of course transcends the aerospace sciences, and unfortunately there is not uniform agreement on semantics. One need only consult the widely cited work of Oreskes, *et al.*[8] to gain an appreciation of the difficulties that arise when definitions are adopted which are less restrictive than those of Roache. Some of the pessimistic conclusions of Ref. 8 should be tempered when Roache's segregation of verification to the mathematical realm and validation to the physical realm is adopted: in this context a suite of potent, though not omnipotent, verification tools does exist; most are based on systematic grid convergence studies. Moreover, in most branches of physical sciences there are well established methods of validation, in the sense of Roache. However, validation is generally agreed to be the more difficult process, as 1) one cannot know *a priori* what physical mechanisms to include in the model, 2) the parameter space is often much too large for a full validation, and 3) some data predicted by the model are inaccessible to measurement or difficult to measure with sufficient precision.

Certainly, it must be understood that exercises associated with both verification and validation provide necessary but insufficient conditions to demonstrate whether the model is properly characterizing physical reality. In that sense, one can consider what we call here verification and validation to be part of the total process that Ref. 8 labels "confirmation," a process in which the veracity of a model is estimated by a series of tests which seek to reduce the probability that the model is false. So indeed while the provocative conclusion of Ref. 8 that "verification and validation of numerical models of natural systems is impossible," is true in a strict logical sense, it does not follow that those exercises called here "verification" and "validation" have no purpose, nor that numerical models do not exist that most sage judges would agree are verified and validated to a high degree of certainty. To the contrary, thousands of successes of the scientific method over the centuries have relied on just such exercises, no matter what their name. Lastly, the arguments raised in Ref. 8 as to how the brand of verification or validation has been used and misused in making decisions ranging from engineering design to public policy have some legitimacy, and only reinforce the notion that our existing language is subject to multiple interpretations in the absence of careful qualification. So, while a satisfactory, universally accepted, and compact linguistic framework is elusive, it is without question that the exercises illustrated in this paper, whatever their name, are a necessary, albeit insufficient, part of a rigorous computational engineering design process.

All that said, it is distressingly easy to find in the literature widespread use of unverified and unvalidated computational predictions, even in the restricted sense of Roache; many of the serious concerns of Ref. 8 would be alleviated had these models passed his stringent, but less encompassing requirements. For example, Powers and Paolucci[9] identify several modern calculations of detonations with detailed chemical kinetics which were predicted on grids that were up to four orders of magnitude too coarse to capture the reaction zone structures intrinsic to the chemistry embodied in mathematical model. In such under-resolved calculations, spurious effects of numerical viscosity are dominant at the finest length scales, and these are likely suppressing potentially important physical effects, especially near physical stability limits.

In the absence of exact solutions, such as for the case studied in Ref. 9, one can still perform verification by first calculating an approximate solution on a fine grid to mimic the exact solution. Then one obtains solutions on coarser grids and checks to see if the differences between the coarse and fine grid solutions are approaching zero at an order of accuracy consistent with the truncation error of the numerical method employed. While this is a necessary condition for verification, it is not sufficient, as the method could be converging to a spurious numerical artifact. Consequently, if possible, it is desirable to check convergence by appeal to an exact solution. There are very few exact solutions for compressible reactive flows with embedded shocks, and their use in verification to date has been minimal.

It is thus the purpose of this paper to give new exact solutions for oblique detonations that can be used for verification, and to provide an example of one such verification. It is noted that the new exact solutions, which will be seen to give predictions entirely consistent with notions which have evolved over the past several decades, do not significantly alter the standard understanding of oblique detonations. Moreover, the significant assumptions required do not render the reduced model appropriate to *quantitatively* describe

an actual laboratory experiment; thus, no validation will be reported here. However, in addition to their utility in verification, there is a pedagogical advantage to be realized in constructing such exact solutions: one learns to distinguish the critical ingredients necessary to achieve an oblique detonation from those that simply provide higher order corrections.

B. Oblique Detonation

An oblique detonation is defined as a shock induced combustion process in which the shock has an angle of inclination to the streamlines of the undisturbed flow. In a detonation, the shock triggers the combustion, and the combustion contributes to the support of the shock. It is generally the case that convective transport dominates diffusive transport. In a typical oblique detonation, an unreacted fluid particle traveling at supersonic velocity in the freestream encounters an oblique shock. Typically, the shock is supported by a stationary downstream solid wedge. As the fluid particle passes through the shock, it is irreversibly compressed such that its temperature rises sufficiently high to induce exothermic reaction. As the particle travels past the shock, it reacts, converting chemical energy into thermal and kinetic energy. This local energy release then propagates via acoustic waves within the domain between the wedge and the shock, and there is a complex series of reflections and interactions. Additionally, the fluid particle turns so that in the far field its pathline is parallel to the supporting wedge. An observable global consequence of this energy release and transport is that the shock is displaced further from the wedge than it otherwise would have been had the flow been inert.

The just-described portrait of an oblique detonation is qualitatively consistent with both experiments and a mathematical theory which has been refined over the past sixty years. Here a small portion of the theoretical literature is reviewed which is most relevant to the present effort. Early analyses focused on the limit of infinitely fast kinetic rates, which allowed an oblique detonation to be modeled by a set of algebraic Rankine-Hugoniot jump conditions with heat release, which gave rise to a prediction of a straight shock attached to a straight wedge. Such an oblique detonation has an infinitely thin reaction zone, and can be thought of as structure-free. Perhaps the first analysis of this type published in the open literature was given by Samaras[10]. Later, Gross[11] improved upon this to obtain a compact and useful representation of the oblique detonation jump state. Pratt, *et al.*'s[12] much later revisitation of the structure-free problem in many ways triggered a renewed interest in oblique detonations for propulsion applications.

In an exothermic analog to the related study of Lee[13], who considered flows with finite rate vibrational relaxation, Powers and Stewart[14] extended the structure-free theory to account for the effects of a single reaction with finite rate kinetics in the limit in which the flow kinetic energy is large relative to the chemical and ambient thermal energies. A special non-orthogonal coordinate system was used to facilitate their asymptotic analysis. Comparisons of the predictions of this theory with those of a standard algorithm for solving the full partial differential equations were given by Grismer and Powers[15] for the case of a curved shock attached to a straight wedge. Using an orthogonal coordinate transformation, Gonthier and Powers[16] extended this theory to account for two finite rate reactions for a straight shock, curved wedge system. Grismer and Powers[17] went on to use an unsteady two-dimensional reactive Euler model to computationally predict stable and unstable oblique detonations with a straight shock and curved wedge.

These verification tools have not been widely utilized in the decade since they appeared. Three factors have likely inhibited the adaptation of the asymptotic solution as a verification benchmark: 1) the asymptotic solution for the curved shock and straight wedge, has an elaborate form, 2) one must use great care to distinguish errors of the asymptotic approximation from numerical truncation errors, and 3) a realization of the often-critical need for verified computational tools, as embodied for example in AIAA standards on numerical accuracy, has not permeated throughout the aerospace community. The present study is an attempt to address these shortcomings.

C. Plan of the Paper

The plan of this paper is as follows. We first describe an unsteady, two-dimensional, inviscid model equivalent to that of Ref. 14. Reaction is described by one-step, irreversible kinetics which allows for reactant depletion to extinguish the reaction. Arrhenius effects are embodied in a Heaviside step function which suppresses reaction before the shock and admits reaction following the shock. Consequently the post-shock reaction is equivalent to an Arrhenius model with zero activation energy. This key assumption allows the equations to be more amenable to analytic solution, and the steady solutions to be less susceptible to instability. Next

an orthogonal coordinate transformation is employed in a manner similar to that used in Ref. 16. The flow is taken to be steady and have spatial variation with only one of the variables in the transformed frame. This, along with the assumption of a straight shock attached to a curved wedge, dictates that the flow is irrotational. The conservation of mass, momentum, and energy equations are then seen to admit algebraic solutions, similar to Rankine-Hugoniot relations, which allows one to express all variables as functions of the extent of reaction. These are deployed in the remaining ordinary differential equation for the reaction kinetics, whose simple form admits then an exact solution giving distance as a function of extent of reaction. Consequently, all flow variables have a parametric expression in terms of the extent of reaction. Next, three limiting cases are studied in which explicit solutions for all variables as functions of position are found: the high Mach number limit, the more robust low heat release limit, and the Chapman-Jouguet (CJ) limit. The exact solution, away from these limits, is then employed for use in verification of a modern computational algorithm for shock-laden reactive flows. It is shown that a third order time-accurate numerical algorithm, which can achieve fifth order spatial accuracy for smooth flows, converges at less than first order spatial accuracy for a flow containing a captured shock. This result is a feature of all shock-capturing schemes and is consistent with the under-appreciated Godunov's theorem[18], derived under slightly more restrictive conditions than apply here.

II. Governing Equations

A. Evolution Axioms and Constitutive Equations

The two-dimensional unsteady reactive Euler equations for a calorically perfect ideal gas which undergoes a single irreversible reaction are expressed in conservative form as

$$\frac{\partial \rho}{\partial t} + \frac{\partial}{\partial x}(\rho u) + \frac{\partial}{\partial y}(\rho v) = 0, \tag{1}$$

$$\frac{\partial}{\partial t}(\rho u) + \frac{\partial}{\partial x}\left(\rho u^2 + p\right) + \frac{\partial}{\partial y}(\rho u v) = 0, \tag{2}$$

$$\frac{\partial}{\partial t}(\rho v) + \frac{\partial}{\partial x}(\rho u v) + \frac{\partial}{\partial y}\left(\rho v^2 + p\right) = 0, \tag{3}$$

$$\frac{\partial}{\partial t}\left(\rho\left(e + \frac{1}{2}(u^2+v^2)\right)\right) + \frac{\partial}{\partial x}\left(\rho u\left(e + \frac{1}{2}(u^2+v^2) + \frac{p}{\rho}\right)\right) + \frac{\partial}{\partial y}\left(\rho v\left(e + \frac{1}{2}(u^2+v^2) + \frac{p}{\rho}\right)\right) = 0, \tag{4}$$

$$\frac{\partial}{\partial t}(\rho\lambda) + \frac{\partial}{\partial x}(\rho u\lambda) + \frac{\partial}{\partial y}(\rho v\lambda) = \alpha\rho(1-\lambda)H(T-T_i), \tag{5}$$

$$e = \frac{1}{\gamma - 1}\frac{p}{\rho} - \lambda q, \tag{6}$$

$$p = \rho R T. \tag{7}$$

Equations (1-7) form a set of seven equations in the seven unknowns ρ, u, v, p, e, λ, and T. Here, as indicated in Fig. 1, the ordinary Cartesian distance coordinates are x and y; while time is t. Dependent variables in Eqs. (1-7) are density ρ, x-velocity u, y-velocity v, pressure p, specific internal energy e, reaction progress λ, and temperature T. Parameters are the reaction kinetic rate constant α, ratio of specific heats γ, heat release per unit mass q, gas constant R, and ignition temperature T_i.

Equations (1-5) are, respectively, expressions of the conservation of mass, x-momentum, y-momentum, and energy, and species evolution. Equation (5) models the irreversible reaction of $A \rightarrow B$ in which species A and B have identical molecular masses and specific heats. The mass fractions of each species, Y_A and Y_B, can be given in terms of the reaction progress variable by the relations $Y_A = 1 - \lambda$ and $Y_B = \lambda$. For a fluid particle which is initially composed exclusively of species A and reacts until it is exclusively composed of species B, one has λ beginning at zero and terminating at unity. The reaction rate is limited by a reactant depletion model, and is proportional to the amount of reactant present. In Eq. (5), $H(T - T_i)$ is a Heaviside step function which suppresses reaction when the temperature is below T_i; this mimics a full Arrhenius model, in which the activation energy is infinite for $T < T_i$ and zero for $T > T_i$. Equations (6-7) are constitutive relations which give the caloric and thermal state equations, respectively.

The standard relations defining the specific heats at constant pressure and volume, c_p and c_v, respectively, are $c_p = \gamma R/(\gamma - 1)$ and $c_v = R/(\gamma - 1)$. Also useful will be the expression for Mach number

$$M = \sqrt{\frac{u^2 + v^2}{\gamma RT}}, \tag{8}$$

and the vorticity ω, which for this two-dimensional flow has only one non-zero scalar component,

$$\omega = \frac{\partial v}{\partial x} - \frac{\partial u}{\partial y}. \tag{9}$$

B. Freestream, Shock, and Boundary Conditions

Here, freestream, shock, and boundary conditions are given for Eqs. (1-7). As only time-independent solutions will be considered, a set of initial conditions is unnecessary. As indicated in Fig. 1, the scenario of a uniform supersonic freestream encountering a straight shock will be modeled. The shock is inclined at an angle β to the horizontal. The freestream variables have values

$$u = u_1, \qquad v = 0, \qquad \rho = \rho_1, \qquad T = T_1, \qquad \lambda = 0. \tag{10}$$

Then by Eq. (7), the ambient pressure is $p_1 = \rho_1 R T_1$, and by Eq. (8), the freestream Mach number is $M_1 = u_1/\sqrt{\gamma R T_1}$.

A standard Rankine-Hugoniot analysis reveals that λ does not jump through a shock discontinuity. This is understandable when one considers that a fluid particle needs a finite amount of time to react, and that it spends an infinitesimally short time traversing the shock jump. The shock jump is taken to be of sufficient strength to raise the temperature above T_i, so as to cause reaction to commence. Thus in the post-shock state, the Heaviside function in Eq. (5) has value unity, and will not be written explicitly from here on. One can also write a detailed set of Rankine-Hugoniot shock jump equations for the other conservation relations; however, since the governing equations are already in the required conservative form, they are entirely consistent with the more general analysis which will follow.

Streamlines $y_s(x)$, which for the steady flow are also particle pathlines, must satisfy the standard equation

$$\frac{dy_s}{dx} = \frac{v}{u}, \tag{11}$$

along with an appropriate initial condition. The shock is assumed to be straight and is taken to be attached to a downstream wall of shape $y = y_w(x)$. The wall shape necessary to induce a straight shock is as of yet unknown, and will be determined as part of the solution procedure. For the inviscid flow, it is not necessary to satisfy a no-slip condition at the downstream wall. It is however necessary to satisfy a kinematic condition which allows no mass flow through the wall surface. This will be guaranteed if the wall surface is coincident with a streamline, so that

$$\frac{dy_w}{dx} = \frac{v}{u}, \qquad y_w(0) = 0, \qquad \text{on} \qquad y = y_w(x). \tag{12}$$

III. Exact Solution

In this section, an exact oblique detonation solution is found which is appropriate for use in verification studies.

A. Rotation of Axes

One first considers the rotation sketched in Fig. 1. Equations (1-5) are invariant under a clockwise rotation of axes through an angle $\pi/2 - \beta$. If $\beta = \pi/2$ is selected, there is no rotation, and all results obtained here will be valid for the important limit of a strictly one-dimensional detonation. The rotation transformation is effected by mapping the vector $\mathbf{x} = (x, y)^T$ to the vector $\mathbf{X} = (X, Y)^T$ by the linear rotation transformation $\mathbf{X} = \mathbf{Q} \cdot \mathbf{x}$:

$$\underbrace{\begin{pmatrix} X \\ Y \end{pmatrix}}_{\mathbf{X}} = \underbrace{\begin{pmatrix} \sin\beta & -\cos\beta \\ \cos\beta & \sin\beta \end{pmatrix}}_{\mathbf{Q}} \underbrace{\begin{pmatrix} x \\ y \end{pmatrix}}_{\mathbf{x}}. \tag{13}$$

Here the transformation matrix $\mathbf{Q}$, often called a rotation matrix, is by construction orthogonal. That is, its columns are composed of orthonormal vectors, its eigenvalues all have value unity, as does its norm. It can be shown then that $\mathbf{Q}^{-1} = \mathbf{Q}^T$ and that the rotation transformation preserves the lengths of vectors: there is no stretching deformation. For invariance, one must also transform velocities from $\mathbf{u} = (u, v)^T$ to $\mathbf{U} = (U, V)^T$ according to the same rotation, $\mathbf{U} = \mathbf{Q} \cdot \mathbf{u}$:

$$\underbrace{\begin{pmatrix} U \\ V \end{pmatrix}}_{\mathbf{U}} = \underbrace{\begin{pmatrix} \sin\beta & -\cos\beta \\ \cos\beta & \sin\beta \end{pmatrix}}_{\mathbf{Q}} \underbrace{\begin{pmatrix} u \\ v \end{pmatrix}}_{\mathbf{u}}. \tag{14}$$

Because of the orthogonality of $\mathbf{Q}$, the inverse transformations for distance and velocity are simply found to be $\mathbf{x} = \mathbf{Q}^{-1} \cdot \mathbf{X} = \mathbf{Q}^T \cdot \mathbf{X}$, and $\mathbf{u} = \mathbf{Q}^{-1} \cdot \mathbf{U} = \mathbf{Q}^T \cdot \mathbf{U}$:

$$\underbrace{\begin{pmatrix} x \\ y \end{pmatrix}}_{\mathbf{x}} = \underbrace{\begin{pmatrix} \sin\beta & \cos\beta \\ -\cos\beta & \sin\beta \end{pmatrix}}_{\mathbf{Q}^T} \underbrace{\begin{pmatrix} X \\ Y \end{pmatrix}}_{\mathbf{X}}, \qquad \underbrace{\begin{pmatrix} u \\ v \end{pmatrix}}_{\mathbf{u}} = \underbrace{\begin{pmatrix} \sin\beta & \cos\beta \\ -\cos\beta & \sin\beta \end{pmatrix}}_{\mathbf{Q}^T} \underbrace{\begin{pmatrix} U \\ V \end{pmatrix}}_{\mathbf{U}}. \tag{15}$$

A critical advantage of such a rotation is that in the rotated frame, the shock locus has the straightforward description $X = 0$. It is also easily seen that magnitudes of distances and velocities are preserved under these transformations; that is, $x^2 + y^2 = X^2 + Y^2$ and $u^2 + v^2 = U^2 + V^2$. Further, scalars such as p, ρ, e, and λ are also invariant under the transformation. Thus, freestream scalars remain unchanged; however, the freestream velocity components transform to $U_1 = u_1 \sin\beta$, $V_1 = u_1 \cos\beta$. Equations for streamlines originating at a generic point on the shock surface $X = 0$, $Y = Y_o$ transform to

$$\frac{dY_s}{dX} = \frac{V}{U}, \qquad Y_s(0) = Y_o. \tag{16}$$

For the streamline at the wall, $Y_o = 0$, and the downstream wall condition, Eq. (12), transforms to

$$\frac{dY_w}{dX} = \frac{V}{U}, \qquad Y_w(0) = 0, \qquad \text{on} \qquad Y = Y_w(X). \tag{17}$$

In the rotated coordinate system, the time-independent version of Eqs. (1-5) is represented as

$$\frac{\partial}{\partial X}(\rho U) + \frac{\partial}{\partial Y}(\rho V) = 0, \tag{18}$$

$$\frac{\partial}{\partial X}\left(\rho U^2 + p\right) + \frac{\partial}{\partial Y}(\rho UV) = 0, \tag{19}$$

$$\frac{\partial}{\partial X}(\rho UV) + \frac{\partial}{\partial Y}\left(\rho V^2 + p\right) = 0, \tag{20}$$

$$\frac{\partial}{\partial X}\left(\rho U\left(e + \frac{1}{2}(U^2+V^2) + \frac{p}{\rho}\right)\right) + \frac{\partial}{\partial Y}\left(\rho V\left(e + \frac{1}{2}(U^2+V^2) + \frac{p}{\rho}\right)\right) = 0, \tag{21}$$

$$\frac{\partial}{\partial X}(\rho U\lambda) + \frac{\partial}{\partial Y}(\rho V\lambda) = \alpha\rho(1-\lambda). \tag{22}$$

Lastly, the vorticity and Mach number transform to

$$\omega = \frac{\partial V}{\partial X} - \frac{\partial U}{\partial Y}, \tag{23}$$

$$M = \sqrt{\frac{U^2+V^2}{\gamma RT}}. \tag{24}$$

B. Extended Rankine-Hugoniot Conditions

Here, a set of algebraic equations which are extensions of the standard Rankine-Hugoniot jump conditions are obtained. In the rotated frame, we seek only solutions which have no variation in Y. Thus, all variables

will be at most a function of X, and the partial derivatives can be replaced with ordinary derivatives to arrive at

$$\frac{d}{dX}\left(\rho U\right) = 0, \tag{25}$$

$$\frac{d}{dX}\left(\rho U^2 + p\right) = 0, \tag{26}$$

$$\frac{d}{dX}\left(\rho U V\right) = 0, \tag{27}$$

$$\frac{d}{dX}\left(\rho U\left(e + \frac{1}{2}(U^2+V^2) + \frac{p}{\rho}\right)\right) = 0, \tag{28}$$

$$\frac{d}{dX}\left(\rho U \lambda\right) = \alpha\rho(1-\lambda). \tag{29}$$

Now, Eqs. (25-28) are homogeneous and can be directly integrated to arrive at a set of equations consistent with Rankine-Hugoniot jump conditions. Doing this, applying freestream conditions, Eq. (10), using Eq. (6) to eliminate e, and using Eq. (25) to simplify Eq. (29), one finds

$$\rho U = \rho_1 u_1 \sin\beta, \tag{30}$$

$$\rho U^2 + p = \rho_1 u_1^2 \sin^2\beta + p_1, \tag{31}$$

$$V = u_1 \cos\beta, \tag{32}$$

$$\frac{\gamma}{\gamma-1}\frac{p}{\rho} - \lambda q + \frac{1}{2}\left(U^2 + u_1^2\cos^2\beta\right) = \frac{\gamma}{\gamma-1}\frac{p_1}{\rho_1} + \frac{1}{2}u_1^2, \tag{33}$$

$$\frac{d\lambda}{dX} = \alpha\frac{1-\lambda}{U}. \tag{34}$$

Equation (32) is consistent with the well known result from inert oblique shock theory that the velocity component tangent to the oblique shock is unchanged through the shock. But here the condition is stronger, as our assumptions give the result that V remains constant throughout the post-shock reactive flow field. Because V is constant and U has no variation with Y by assumption, Eq. (23) holds that the entire post-shock flow field must be irrotational: $\omega = 0$.

Equations (30-33) have full equivalents in Refs. 10-12, 14 and 16, albeit in slightly different notation. Now Eqs. (30-31, 33) constitute three non-linear algebraic equations in the four unknowns ρ, U, p, and λ. A lengthy series of operations on these equations leads one to form explicit algebraic expressions for $\rho(\lambda)$:

$$\rho(\lambda) = \frac{\rho_1(\gamma+1)M_1^2\sin^2\beta}{1+\gamma M_1^2\sin^2\beta \pm \sqrt{\left(1+\gamma M_1^2\sin^2\beta\right)^2 - (\gamma+1)M_1^2\sin^2\beta\left(2 + \frac{\gamma-1}{\gamma}\frac{2\lambda q}{RT_1} + (\gamma-1)M_1^2\sin^2\beta\right)}}. \tag{35}$$

Now for a physical density prediction, the term inside the radical in Eq. (35) must be non-negative for $\lambda \in [0,1]$. Algebraic analysis reveals that this condition will hold if

$$q \leq \frac{\gamma R T_1 (M_1^2\sin^2\beta - 1)^2}{2(\gamma^2-1)M_1^2\sin^2\beta}. \tag{36}$$

When the equality holds, the condition is the two-dimensional equivalent of a CJ detonation. The CJ oblique detonation given by this model can be shown to predict a locally sonic component of velocity normal to the oblique shock at the point of complete reaction ($\lambda = 1$).

It can be shown that the "+" solution of Eq. (35) is associated with the unshocked branch and the "-" solution is associated with the shocked branch. More specifically, when $\lambda = 0$, the "+" solution is the ambient density ρ_1, and the "-" solution is the classical inert oblique shock solution. As the unshocked branch has no clear mechanism to trigger ignition, it will be discarded from here on. The shocked "-" branch of Eq. (35) is valid for the domain between the shock and the confining wall. It is a function of known freestream parameters and the as of yet unknown function $\lambda(X)$. Other variables are then easy to calculate. For example, using Eqs. (30-31) one obtains

$$U(\lambda) = \frac{\rho_1 u_1 \sin\beta}{\rho(\lambda)}, \tag{37}$$

$$p(\lambda) = p_1 + \rho_1^2 u_1^2 \sin^2\beta \left(\frac{1}{\rho_1} - \frac{1}{\rho(\lambda)}\right), \tag{38}$$

$$T(\lambda) = \frac{p_1}{\rho(\lambda)R} + \frac{\rho_1^2 u_1^2 \sin^2\beta}{\rho(\lambda)R}\left(\frac{1}{\rho_1} - \frac{1}{\rho(\lambda)}\right). \tag{39}$$

C. Reaction Zone Structure Solution

Now, the necessary ingredients are available for integration of Eq. (34). Employing Eq. (37), Eq. (34) can be rewritten as

$$\frac{d\lambda}{dX} = \frac{\alpha}{\rho_1 u_1 \sin\beta}\ \rho(\lambda)(1-\lambda), \qquad \lambda(0) = 0, \tag{40}$$

where $\rho(\lambda)$ is taken from the shocked "-" branch of Eq. (35). Next separation of variables allows Eq. (40) to be integrated to form an exact solution for $X(\lambda)$:

$$X(\lambda) = a_1\left(2a_3\left(\sqrt{1-a_4\lambda}-1\right) + \ln\left(\left(\frac{1}{1-\lambda}\right)^{a_2}\left(\frac{\left(1-\sqrt{\frac{1-a_4\lambda}{1-a_4}}\right)\left(1+\sqrt{\frac{1}{1-a_4}}\right)}{\left(1+\sqrt{\frac{1-a_4\lambda}{1-a_4}}\right)\left(1-\sqrt{\frac{1}{1-a_4}}\right)}\right)^{a_3\sqrt{1-a_4}}\right)\right), \tag{41}$$

where the intermediate parameters $a_1, \ldots, a_4$ have the definitions

$$a_1 = \frac{1}{(\gamma+1)M_1\sin\beta}\frac{\sqrt{\gamma R T_1}}{\alpha}, \tag{42}$$

$$a_2 = 1 + \gamma M_1^2 \sin^2\beta, \tag{43}$$

$$a_3 = M_1^2\sin^2\beta - 1, \tag{44}$$

$$a_4 = 2\frac{M_1^2\sin^2\beta}{\left(M_1^2\sin^2\beta - 1\right)^2}\frac{\gamma^2-1}{\gamma}\frac{q}{RT_1}. \tag{45}$$

Note that a_1 has units of length while a_2, a_3, and a_4 are dimensionless. When $a_4 < 1$, Eq. (36) is satisfied, and Eq. (41) predicts a real solution. For $a_4 = 1$, a CJ oblique detonation is predicted. If $a_4 > 1$, Eq. (36) is violated, and complex values of X are predicted. Numerical experiments on Eq. (41) indicate that for $\lambda \in [0,1]$ that $X(\lambda)$ is single valued and monotonically increasing with λ. When non-physical large negative values of λ are considered, the function can be multivalued.

One can find the locus of a generic streamline Y_s originating at the shock surface $X = 0$, $Y = Y_o$ as a function of λ. Scaling Eq. (16) by Eq. (34) and employing Eq. (32), one gets

$$\frac{dY_s}{d\lambda} = \frac{u_1\cos\beta}{\alpha}\frac{1}{1-\lambda}, \qquad Y_s(\lambda = 0) = Y_o. \tag{46}$$

Solving, one gets

$$Y_s(\lambda) = \frac{u_1\cos\beta}{\alpha}\ln\left(\frac{1}{1-\lambda}\right) + Y_o. \tag{47}$$

For the streamline originating at the wall $Y_o = 0$, so the wall shape is given by

$$Y_w(\lambda) = \frac{u_1\cos\beta}{\alpha}\ln\left(\frac{1}{1-\lambda}\right). \tag{48}$$

Last, since the flow is irrotational, a velocity potential exists. The velocity potential ϕ is defined such that

$$\frac{\partial\phi}{\partial X} = U, \tag{49}$$

$$\frac{\partial\phi}{\partial Y} = V. \tag{50}$$

Now dividing both sides of Eq. (49) by both sides of Eq. (34), one gets

$$\frac{\partial\phi}{\partial\lambda} = \frac{1}{\alpha}\frac{U^2(\lambda)}{1-\lambda}. \tag{51}$$

Integrating, one gets

$$\phi(X,Y) = \frac{1}{\alpha}\int_0^{\lambda(X)} \frac{U^2(s)}{1-s}\, ds + f(Y), \tag{52}$$

where s is a dummy variable and $f(Y)$ is a function of Y. Now since $\partial\phi/\partial Y = V = u_1 \cos\beta$, one finds $df/dY = u_1 \cos\beta$, so $f(Y) = (u_1 \cos\beta)\, Y + \phi_o$, where ϕ_o is an arbitrary constant which can be set to zero. So the velocity potential is given by

$$\phi(X,Y) = \frac{1}{\alpha}\int_0^{\lambda(X)} \frac{U^2(s)}{1-s}\, ds + (u_1 \cos\beta)\, Y. \tag{53}$$

D. Predictions of the Exact Solution

A simple test case is studied for a set of parameter values listed in Table 1. The numbers here are in infinite precision to facilitate the formal verification. The larger the value of q that is employed, the easier it is to visualize the effects of the heat release on the flow field. Here $q = 300000\ J/kg$ meets the additional restriction of Eq. (36) which for the parameters of Table 1 demand that $q \leq 3515750/11\ J/kg$; using the nomenclature described in Ref. 16, this is an example of a weak overdriven oblique detonation. For $q > 3515750/11\ J/kg$, a different class of flow topology would be predicted. For straightforward implementation into industrial codes, all parameters and results reported here are dimensional. These parameters, while somewhat arbitrary, are not unreasonable for common gases that may be operating in a high speed propulsion device. In particular they were chosen so that the global reaction zone lengths were on the order of 1 m, and that significant variation in flow variables, such as ρ and T, could be predicted throughout the reaction zone. It should be remembered, however, that the purpose of this paper is to develop a useful verification methodology utilizing the new exact solution; consequently, more flexibility in parameter choices is exercised relevant to the equally important, but distinct, task of validation relative to actual experiments.

In Fig. 2, a plot is given of various flow variables: a) reaction progress, b) density, c) temperature, and d) Mach number in the direction normal to the shock, as functions of the normal distance from the shock, X. Figure 2a demonstrates that reaction progress is zero until the shock at $X = 0\ m$ is reached. At the shock, there is no jump in λ, while there is a jump in its derivative. The irreversible reaction induces a relaxation of λ to unity near $X = 0.6\ m$. Fig. 2b shows the variation of density. Here the shock jump is clearly seen at $X = 0\ m$, followed by a relaxation to equilibrium in the reaction zone. In Fig. 2c, the temperature is seen to jump from its ambient value to over 423 K, which is followed by a further increase as heat is released till it reaches an equilibrium value of near 567 K. The Mach number in the direction normal to the wave is initially supersonic at $M_X = 3$. The shock jump reduces it to a subsonic state, and then it increases through the reaction zone to a final value of 0.862. Thus, this oblique detonation is, using nomenclature of Ref. 16, weak, in the sense of an oblique shock, and overdriven, in the sense of a detonation.

In Fig. 3 a plot is given of the streamlines and oblique shock wave for the oblique detonation flow field. Also shown is the locus of points near where the reaction progress has advanced to $\lambda \sim 0.9$, located at $X = 0.665\ m$. For use in a detailed flow verification of a computational code, a set of benchmark values along the wall streamline are given in Table 2. To perform a high precision verification, as is reported later in this paper, many more points need to be considered. The truncated set given here simply provides the reader interested in performing independent verifications another means to check results. While these predictions are valid for a single streamline, one can construct the entire flow field by translating each streamline to a different origin on the oblique shock. This is a consequence of the solution only retaining variation in the X direction in the rotated coordinate system.

IV. Limiting Case Solutions

Here the exact solution is studied in three limiting cases: A) the high Mach number limit, B) the low heat release limit, and C) the Chapman-Jouguet limit.

A. High Mach Number Limit

In the limit of large M_1, one can obtain asymptotic expressions for all variables as explicit functions of X. While these will offer some advantage over the parametric formulæ given in the previous section, it will be

seen that the high sensitivity of the asymptotic solution to the choice of parameters renders it more difficult to use as a verification tool.

Expanding Eqs. (35, 37-39) in the limit as $1/M_1 \to 0$ yields

$$\frac{\rho(\lambda)}{\rho_1} = \frac{\gamma+1}{\gamma-1}\left(1 - \frac{1}{M_1^2 \sin^2\beta}\frac{\gamma+1}{\gamma}\left(\frac{2\gamma}{\gamma^2-1} + \frac{\lambda q}{RT_1}\right) + O\left(\frac{1}{M_1^4}\right)\right), \tag{54}$$

$$\frac{U(\lambda)}{u_1 \sin\beta} = \frac{\gamma-1}{\gamma+1}\left(1 + \frac{1}{M_1^2 \sin^2\beta}\frac{\gamma+1}{\gamma}\left(\frac{2\gamma}{\gamma^2-1} + \frac{\lambda q}{RT_1}\right) + O\left(\frac{1}{M_1^4}\right)\right), \tag{55}$$

$$\frac{p(\lambda)}{p_1} = M_1^2 \sin^2\beta \frac{2\gamma}{\gamma+1}\left(1 - \frac{1}{M_1^2 \sin^2\beta}\frac{\gamma^2-1}{2\gamma}\left(\frac{1}{\gamma+1} + \frac{\lambda q}{RT_1}\right) + O\left(\frac{1}{M_1^4}\right)\right). \tag{56}$$

$$\frac{T(\lambda)}{T_1} = M_1^2 \sin^2\beta \frac{2\gamma(\gamma-1)}{(\gamma+1)^2}\left(1 + \frac{1}{M_1^2 \sin^2\beta}\frac{(\gamma+1)(3-\gamma)}{2\gamma}\left(\frac{-1+6\gamma-\gamma^2}{(\gamma^2-1)(3-\gamma)} + \frac{\lambda q}{RT_1}\right) + O\left(\frac{1}{M_1^4}\right)\right). \tag{57}$$

A similar procedure can be used to find estimates for other variables.

Equations (54-57) can easily be shown to be equivalent to formulæ presented in Ref. 14, and reduce to known equations for high Mach number inert oblique shocks when $q = 0$; for example, equivalent leading order inert approximations are given by Anderson.[21] Moreover, Eq. (54) predicts ρ to decrease after the shock as λ, and thus X, increase, which is in qualitative agreement with the predictions of the exact theory as seen in Fig. 2b. Similarly, the prediction of Eq. (57) for T to increase with λ and thus X is consistent with the exact theory as predicted in Fig. 2c. And though not shown in Fig. 2, the asymptotic theory qualitatively agrees with the exact solution in predicting U to increase and p to decrease after the shock. Thus, consideration of this asymptotic limit allows one to have further confidence that the parent exact solution is the correct one.

However, care must be used in interpreting asymptotic results, formally valid in the limit as $M_1 \to \infty$, for finite values of M_1. For example, using the parameters of Table 1, Eq. (54) predicts a non-physical, negative value for density at complete reaction, which obviously implies larger Mach numbers need to be considered, in this case $M_1 > 5.73$, in order for the asymptotic theory to have even rudimentary physical viability. Moreover, consistent with the result found in Ref. 15 for slightly different parameter values, to insure the asymptotic prediction is truly in the convergent regime, one actually demands $M_1 \geq 20$. For such high Mach numbers, additional care must be exercised to distinguish numerical truncation errors from errors in the asymptotic theory; furthermore, the connection to physical reality becomes more tenuous as neglected physical mechanisms such as real gas effects often have prominence at these high Mach numbers. Of course the verification process is oblivious to whether or not real gas effects have been included. But in order to convince a skeptical audience of the utility of verification, it is useful to inasmuch as possible to consider parameter ranges which approximate those of real physical systems.

Now the high Mach number limit theory provides an estimate of the error; for the predictions of Eqs. (54-57), the error should be of $O(1/M_1^4)$. Formally then, one requires that in the limit of large M_1 that the difference between the exact and high Mach number asymptotic predictions, scaled by $1/M_1^4$ approach a constant value. For the parameters of Table 1, calculation shows that $\lim_{M_1\to\infty}(\rho_e - \rho_a)M_1^4/\rho_1 = -11356.201$. Here ρ_e is the density predicted by the exact Eq. (35) and ρ_a is that predicted by the approximate Eq. (54) in the limit $\lambda \to 1$. While it is atypical that the constant to which the scaled difference relaxes is so high, it is all that is required of an asymptotic theory, and it has been verified for even absurdly high values of M_1 by infinite precision computer algebra calculations. The high magnitude of this constant limits the utility of the high Mach number limit solution.

The leading order equation for the reaction zone structure is found by substituting the leading order portion of Eq. (54) into Eq. (40) to get

$$\frac{d\lambda}{dX} = \frac{\alpha}{u_1 \sin\beta}\frac{\gamma+1}{\gamma-1}(1-\lambda), \qquad \lambda(0) = 0. \tag{58}$$

Solving, one gets

$$\lambda(X) = 1 - \exp\left(-\frac{(\gamma+1)\alpha}{(\gamma-1)u_1 \sin\beta}X\right) \tag{59}$$

Obviously $\lambda \to 1$ as $X \to \infty$. Equation (59) can be substituted into Eqs. (54-57) to get explicit expressions for $\rho(X)$, $U(x)$, $p(X)$, and $T(X)$ valid as $M_1 \to \infty$.

The relaxation length at leading order, X_r, is easily seen from Eq. (59) to be

$$X_r \sim \frac{\gamma-1}{\gamma+1}\frac{u_1 \sin\beta}{\alpha}. \tag{60}$$

It is proportional to the post shock particle velocity and inversely proportional to the kinetic rate constant. At $X = X_r$, the high Mach number theory predicts λ to have increased to $e^{-1} \sim 0.368$. For the parameters of Table 1, the high Mach number theory predicts a relaxation length of $X_r = 0.062\ m$, which agrees moderately well with the predictions of the exact solution seen in Table 2, at which distance λ acquires a value of 0.248. The agreement worsens downstream. At $X = 3X_r = 0.186\ m$, the high Mach number theory predicts $\lambda = 0.950$, while Table 2 shows the exact solution predicts $\lambda \sim 0.538$ at the same point. A comparison of the predictions of the exact and high Mach number theories for this parameter choice is given in Fig. 4. The only modest agreement here is a consequence of $M_1 = 3$ being too small for the high Mach number asymptotic prediction to be highly accurate.

At leading order, the velocity potential can be determined by substituting the leading order portion of Eq. (55) and Eq. (59) into Eq. (53) and integrating to get

$$\phi(X,Y) = \frac{\gamma-1}{\gamma+1}(u_1 \sin\beta)X + (u_1 \cos\beta)Y + O\left(\frac{1}{M_1^2}\right). \tag{61}$$

Lines of constant potential have slope in X, Y space of $-\tan\beta(\gamma-1)/(\gamma+1)$. At leading order, the wall shape can be determined by using Eq. (59) to eliminate λ in Eq. (48) so as to get, after simplification,

$$Y_w(X) = \frac{\gamma+1}{\gamma-1}\frac{1}{\tan\beta}X + O\left(\frac{1}{M_1^2}\right). \tag{62}$$

At leading order, the wall shape is a straight line, whose slope is the negative reciprocal of equipotential lines. Hence the wall streamline is orthogonal to equipotential lines. Using Eq. (13) to transform Eq. (62) back to unrotated Cartesian coordinates, one finds

$$y_w(x) = \left(\frac{\frac{1}{\sin\beta}\frac{\gamma+1}{\gamma-1}\tan\beta - 1}{\tan\beta + \frac{1}{\sin\beta}\frac{\gamma+1}{\gamma-1}}\right)x + O\left(\frac{1}{M_1^2}\right). \tag{63}$$

At leading order, this straight wall has an angle of inclination θ to the horizontal of

$$\theta = \tan^{-1}\left(\frac{y_w}{x}\right) = \tan^{-1}\left(\frac{\frac{1}{\sin\beta}\frac{\gamma+1}{\gamma-1}\tan\beta - 1}{\tan\beta + \frac{1}{\sin\beta}\frac{\gamma+1}{\gamma-1}}\right). \tag{64}$$

In the further limit as $\beta \to 0$, Eq. (64) reduces to the classical thin airfoil limit result[21]: $\beta \sim (\gamma+1)\theta/2$. Lastly in a result from Ref. 14, one can show in the limit as $M_1 \to \infty$ that in order to prevent the shock from becoming detached from the wedge that one must demand $\theta \leq \sin^{-1}(1/\gamma)$, and $\beta \leq \sin^{-1}\sqrt{(\gamma+1)/(2\gamma)}$. For $\gamma = 6/5$, this corresponds to constraints on wedge and shock angles of $\theta \leq 56.4°$, and $\beta \leq 73.2°$, respectively.

B. Low Heat Release Limit

When Eq. (41) is considered in the limit of small, finite heat release, $a_4 \to 0$, it simplifies considerably, to take on the form

$$X(\lambda) = a_1\left(a_5 \ln(1-\lambda) - \frac{a_3 a_4}{2}\lambda\right). \tag{65}$$

Here the new constant parameter a_5 is defined by

$$a_5 = a_3 - a_2 - \frac{a_3 a_4}{2}. \tag{66}$$

Next, Eq. (65) can be inverted to form

$$\lambda(X) = 1 - \frac{2a_5}{a_3 a_4} W_0\left[\frac{a_3 a_4}{2a_5}\exp\left(\frac{X}{a_1 a_5} + \frac{a_3 a_4}{2a_5}\right)\right]. \tag{67}$$

Here, $W_0(s)$ is the principal branch of the Lambert W function[19,20], of the dummy variable s. When $s = we^w$, $W(s) = w$, where w is also a dummy variable; consequently, W can be thought of as an extended logarithm, sometimes called the "product log." For $s \in [-e^{-1}, 0]$, as the argument is in Eq. (67), $W(s)$ is dual-valued with both values negative. The principal branch, $W_0(s)$, is taken as the branch which has an analytic continuation through the origin. On the principal branch $s \in [-e^{-1}, 0]$ maps to $W_0 \in [-1, 0]$. The alternate branch $W_{-1}(s)$ is the branch which has an analytic continuation to negative infinity and maps $s \in [-e^{-1}, 0]$ onto $W_{-1} \in [-1, -\infty)$. For $s > 0$, $W(s)$ is single-valued, and for $s < -e^{-1}$, $W(s)$ has no real value. With $\lambda(X)$ from Eq. (67), it is easy to predict the variation of other flow variables using Eqs. (35,37-39).

An improved estimate of the reaction zone thickness is found from Eq. (67) by setting $X_r \sim -a_1 a_5$. Using the definitions of Eqs. (42-45,66), one finds then

$$X_r \sim \frac{\gamma - 1}{\gamma + 1} \frac{u_1 \sin\beta}{\alpha} \left(1 + \frac{2}{(\gamma - 1) M_1^2 \sin^2\beta} + \frac{\gamma + 1}{\gamma (M_1^2 \sin^2\beta - 1)} \frac{q}{RT_1} \right). \tag{68}$$

Equation (68) gives a correction to Eq. (60) for finite Mach number and heat release effects. For the parameters of Table 1, Eq. (68) predicts a reaction zone thickness of $X_r \sim 0.313\ m$, which agrees well with the predictions of the exact solution seen in Table 2, at which distance λ acquires a value of 0.704. Figure 4 also includes a comparison of the predictions of improved approximation of Eq. (67) against those of the exact Eq. (41) for the conditions of Table 1. The improved prediction is good and yields a slight over-prediction of λ at a given value of X.

C. CJ Limit

When the flow conditions are such that $a_4 = 1$, the oblique detonation has a CJ character. The flow at the end of such a reaction zone is locally sonic; moreover, one set of characteristic curves becomes parallel to the shock wave. In a one-dimensional flow with one-step irreversible kinetics, the CJ velocity can be shown to be the velocity of an unsupported wave, and thus it has an important physical significance. In contrast, there is no particular tendency for most oblique detonations to relax to the CJ state; in practice, they are usually overdriven. Nevertheless, for completeness, and because a result is obtained which is useful in the one-dimensional limit, $\beta \to \pi/2$, a brief characterization of the CJ state is given here.

For $a_4 = 1$, Eq. (41) reduces considerably to

$$X_{CJ}(\lambda) = -a_1 \left(2a_3 \left(1 - \sqrt{1 - \lambda} \right) + a_2 \ln(1 - \lambda) \right). \tag{69}$$

Equation (69) can be inverted to form an explicit expression for $\lambda_{CJ}(X)$:

$$\lambda_{CJ}(X) = 1 - \left(\frac{a_2}{a_3} W_0 \left[-\frac{a_3}{a_2} \exp\left(-\frac{X}{2a_1 a_2} - \frac{a_3}{a_2} \right) \right] \right)^2. \tag{70}$$

With $\lambda_{CJ}(X)$ from Eq. (70), it is easy to predict the variation of other flow variables under CJ conditions using Eqs. (35,37-39). The CJ reaction zone thickness is estimated by taking $X_{rCJ} \sim 2a_1 a_2$. Using Eqs.(42,43), this reduces to

$$X_{rCJ} \sim \frac{2\gamma}{\gamma + 1} \frac{u_1 \sin\beta}{\alpha} \left(1 + \frac{1}{\gamma M_1^2 \sin^2\beta} \right). \tag{71}$$

Last one notes that when $a_4 = 1$, that M_1 and q are no longer independent by Eq. (45). Solving for M_1 in terms of q for the CJ limit gives rise to a quartic equation, which has four complicated solutions for left and right running CJ deflagrations and detonations.

V. Computational Solution

This section describes computational solutions in the spatio-temporal domain $x \in [-0.25\ m, 1.75\ m]$, $y \in [0\ m, 2\ m]$, $t \in [0\ s, 0.01\ s]$.

A. Numerical Algorithm

The numerical method employs a uniform Cartesian grid, with an internal boundary method to handle the curved wall boundary condition. The internal boundary is represented by a level set function, $\psi = 0$,

where $\psi > 0$ in the boundary region, and $\psi < 0$ in the flow region. The spatial discretization scheme is based on the nominally fifth order weighted essentially non-oscillatory shock-capturing scheme of Jiang and Shu[22], in conjunction with a non-decomposition based Lax-Friedrichs solver. For temporal discretization, a third order Runge-Kutta time integration technique is used. The details are fully described in Xu, *et al.*[23] It is emphasized that the fifth order spatial accuracy can only be realized for flows which contain no discontinuities, unlike those of this study. The physical parameters used in the computation are those in Table 1. In addition, the ignition temperature, T_i, is chosen to be halfway between the freestream and shock temperature, $T_i = 361.58\ K$.

B. Error Norm, Initial Conditions and Time Integration

For verification, the exact solution must be compared with the computed one. When flows contain captured shocks, it is important to measure error using a norm such as L_1; for obvious reasons, shock-capturing solutions will not converge in the L_∞ norm. The error in density, using an L_1 norm, is denoted by

$$L_1 = \sum_{i=0}^{N} \sum_{j=0}^{N} H(-\psi_{ij}) |\rho_{n,ij} - \rho_{e,ij}| \Delta x \Delta y, \tag{72}$$

where ρ_n and ρ_e are the numerical and exact value of density, i and j are the grid indices, and $N+1$ is the number of points in either direction. Note that L_1, as defined, is dimensional with units of density $\times$ area. In all cases uniform grid sizes are utilized with $\Delta x = \Delta y$; from here on, only values for Δx will be reported. Here $H(-\psi_{ij})$ is the Heaviside function, and is used so that errors are only measured in the flow region.

Since a time-dependent numerical algorithm is being used, initial conditions also need to be specified. These are simply given by the freestream conditions. When comparing a time-dependent numerical solution to a steady exact solution, it is imperative to consider a final time which is large enough to relax all physical transients. However, the computational predictions will never be *exactly* steady, so the modeler must exercise some discretion in choosing when to terminate the calculation. In practice, it is not difficult to discern an appropriate cut-off time. It is also noted, making an inference from the study of Short and Stewart[24], that it is likely that the exact physical solution is linearly stable to small perturbations because the zero activation energy case has been taken. So, when the time-dependent solution is near the steady, exact solution, all modes should decay exponentially in time to the steady, exact solution. So, for this problem, L_1 can be tracked as a function of time, and the solution is steady when L_1 is no longer significantly changing.

C. Predictions of the Computational Algorithm

A comparison of exact and long time computed density contours is made in Fig. 5. Here a spatial discretization of $\Delta x = 1/128\ m$ was employed. There is good agreement between the predictions of the two methods. Figure 6 gives the L_1 residual in ρ as time advances for various spatial resolutions from $\Delta x = 1/32\ m$ to $\Delta x = 1/512\ m$. The residuals, for all spatial resolutions, decrease rapidly at early time, and at nearly the same rate. When the residual starts to become time-independent, and thus represent the steady state error, is a function of spatial resolution. This is because the finer grid resolutions can faithfully track the time-dependent decaying modes further in time before being overwhelmed by the spatial inaccuracies. For example, the $\Delta x = 1/32\ m$ calculation appears to be steady around $t \approx 0.005\ s$, while the $\Delta x = 1/512\ m$ calculation is not steady until $t \approx 0.006\ s$. Figure 7 displays the L_1 error in density, at long time, versus grid discretization length. From this plot, it is determined that the approximate rate of convergence in density is $O(\Delta x^{0.779})$, nearly, but not quite, first order. The errors in other field variables show similar trends. The sub-first order convergence is typical of shock-capturing schemes where linearly degenerate characteristics exist, but is often missed when reporting convergence rates.

VI. Discussion

A new exact solution for steady two-dimensional compressible reactive flow with a leading shock followed by a finite length reaction zone has been obtained. Exact solutions for flows of this class are rare and have principal utility as benchmarks for verification of the predictions of computational codes. Here, with the employment of a modern shock-capturing code, an unambiguous example of a verification has been provided; it is emphasized that the verification is in the sense of Roache, which implies only that there is a

high probability that the numerical method is capturing the essence of a true mathematical solution of the governing equations. The exact solution has a simpler representation in the asymptotic limit of high Mach number. However, in the range of parameter space studied, this solution has limited value as a benchmark because it is far from the convergent regime. This does not preclude a more limited value of the high Mach number solution as a representation which more clearly explicates the qualitative dependency of the solution on the flow variables and serves as another useful check on the character of the mathematical solution in that it can be compared with the predictions of an inert theory in the same limits. When the high Mach number results are extended to better account for finite heat release, the predictions become much better, at the expense of a more complicated algebraic expression in terms of the transcendental Lambert W function.

The spatial resolution convergence study necessary for verification gives results consistent with Godunov's theorem which holds that *linear monotonicity-preserving methods are first order accurate at best.*[18,25] While the high order method employed here does not satisfy all the conditions of Godunov's theorem, the $O(1)$ error introduced near captured discontinuities convects throughout the entire domain, giving rise to a method which is at most $O(\Delta x)$ accurate *globally*. Thus, for flows with embedded discontinuities, the fastest any error norm converges to zero is at a rate which is linear with the size of the grid discretization, even if, based on Taylor series estimates which presume continuity, the spatial discretization gives a higher order estimate of spatial accuracy. Moreover, depending on the details of the problem, the realized convergence rate is often worse than linear. Consequently, enthusiasm displayed by some practitioners for employing high-order spatial discretizations in a shock-capturing method for hyperbolic problems should be appropriately restrained: grid resolution studies reveal predictions of nominally high order methods are often only marginally better than simpler nominally first order methods such as Lax-Friedrichs.

While this pessimistic convergence result has long been recognized in many quarters, it is more often unrecognized. The casual reader of much of the best literature for solving hyperbolic systems, including the outstanding monographs of Laney[25] or LeVeque[26], as well as a large fraction of the modern shock-capturing literature, would be hard pressed to come away with a realization that highly touted high order methods simply do not converge with the suggested rapidity for flows with embedded discontinuities. The common technique of comparing predictions of methods in side by side graphs in which large variations are readily seen is useful at a qualitative level, but no substitute for often neglected grid convergence studies. Such exercises provide an ideal way to satisfy the AIAA policy on numerical accuracy. As an alternative, advocates of spectral methods[27,28], while generally avoiding problems with discontinuities, have systematically incorporated grid resolution into their work, and the shock-capturing community would benefit from an analogous effort. Moreover, one can turn to studies from the shock fitting literature to find convergence rates consistent with the nominal order of the discretization method. For example, the recent study of Brooks and Powers[29] shows spectral convergence to machine accuracy on a coarse 65×33 grid for a blunt body re-entry problem, and the results of Henrick, *et al.*[30] exhibit true fifth order accuracy which gives rise to predictions of detonation instabilities which agree remarkably well with those of linear stability theory.

The spatial convergence study illustrates another useful point regarding length scales. In the problem studied here, there is one intrinsic physical length scale: X_r, the reaction zone length scale. There is a second length scale which is a numerical relic of the particular discretization scheme employed. This can be labeled an artificial viscous length scale. This scale is inherent to all shock-capturing schemes, no matter what the order and is a monotonically increasing function of discretization length; however, different schemes will predict different artificial viscous length scales. Whatever the numerical scheme, the calculation can only be verified when the grid is sufficiently fine to insure the length scale associated with artificial viscosity is far less than the reaction zone length scale. When this condition is met, one will predict the error norm to be converging at a rate consistent with Godunov's theorem, and the algorithm can be said to be verified in the sense of Roache. As a counter-example detailed in a companion paper[9], nearly all of the widespread modern detonation calculations with detailed kinetics are unverified, have unresolved reaction zone structures at the finest scales, and allow artificial viscous effects to overwhelm physical effects which are claimed to be modeled. The consequences of this need be determined for a properly skeptical general community to have trust in the predictions of computational modelers.

Acknowledgment

This study was performed under the auspices of the U. S. Department of Energy.

References

[1] Oberkampf, W. L., and Trucano, T. G., "Verification and Validation in Computational Fluid Dynamics," *Progress in Aerospace Sciences*, Vol. 38, No. 3, 2002, pp. 209-272.

[2] Oberkampf, W. L, and Blottner, F. G., "Issues in Computational Fluid Dynamics Code Verification and Validation," *AIAA Journal*, Vol. 36, No. 5, 1998, pp. 687-695.

[3] Roache, P. J., "Quantification of Uncertainty in Computational Fluid Dynamics," *Annual Review of Fluid Mechanics*, Vol. 29, 1997, pp. 123-160.

[4] Roache, P. J., *Verification and Validation in Computational Science and Engineering*, Hermosa, Albuquerque, NM, 1998.

[5] Roache, P. J., "Verification of Codes and Calculations," *AIAA Journal*, Vol. 36, No. 5, 1998, pp. 696-702.

[6] Roache, P. J., "Code Verification by the Method of Manufactured Solutions," *Journal of Fluids Engineering*, Vol. 124, No. 1, 2002, pp. 4-10.

[7] Roache, P. J., "Building PDE Codes to be Verifiable and Validatable," *Computing in Science and Engineering*, Vol. 6, No. 5, 2004, pp. 30-38.

[8] Oreskes, N., Shrader-Frechette, K., and Belitz, K., "Verification, Validation, and Confirmation of Numerical Models in the Earth Sciences," *Science*, Vol. 263, No. 5147, 1994, pp. 641-464.

[9] Powers, J. M., and Paolucci, S., "Accurate Estimates of Fine Scale Reaction Zone Thicknesses in Gas Phase Detonations," AIAA Paper 2005-1171, Jan. 2005, (submitted to the *AIAA Journal*).

[10] Samaras, D. G., "Gas Dynamic Treatment of Exothermic and Endothermic Discontinuities," *Canadian Journal of Research A*, Vol. 26, No. 1, 1948, pp. 1-21.

[11] Gross, R. A., "Oblique Detonation Waves," *AIAA Journal*, Vol. 1, No. 5, 1963, pp. 1225-1227.

[12] Pratt, D. T., Humphrey, J. W., and Glenn, D. E., "Morphology of Standing Oblique Detonation Waves," *Journal of Propulsion and Power*, Vol. 7, No. 5, 1991, pp. 837-645.

[13] Lee, R. S., "A Unified Analysis of Supersonic Nonequilibrium Flow over a Wedge: I. Vibrational Nonequilibrium," *AIAA Journal*, Vol. 4, No. 1, 1966, pp. 30-37.

[14] Powers, J. M., and Stewart, D. S., "Approximate Solutions for Oblique Detonations in the Hypersonic Limit," *AIAA Journal*, Vol. 30, No. 3, 1992, pp. 726-736.

[15] Grismer, M. J., and Powers, J. M., "Comparisons of Numerical Oblique Detonation Solutions with an Asymptotic Benchmark," *AIAA Journal*, Vol. 30, No. 12, 1992, pp. 2985-2987.

[16] Powers, J. M., and Gonthier, K. A., "Reaction Zone Stuctures for Strong, Weak Overdriven, and Weak Underdriven Oblique Detonations," *Physics of Fluids A*, Vol. 4, No. 9, 1992, pp. 2082-2089.

[17] Grismer, M. J., and Powers, J. M., "Numerical Predictions of Oblique Detonation Stability Boundaries," *Shock Waves*, Vol. 6, No. 3, 1996, pp. 147-156.

[18] Godunov, S. K., "A Difference Scheme for Numerical Computation of Discontinuous Solutions of Hydrodynamic Equations," *Matematicheskii Sbornik*, Vol. 47, 1959, pp. 271-306. English translation in U.S. Joint Publications Research Service, JPRS 7226, 1969.

[19] Corless, R. M., Gonnet, G. H., Hare, D. E. G., Jeffrey, D. J., and Knuth, D. E., "On the Lambert W Function," *Advances in Computational Mathematics*, Vol. 5, No. 4, 1996, pp. 329-359.

[20] Borwein, J. M., and Corless, R. M., "Emerging Tools for Experimental Mathematics," *American Mathematical Monthly*, Vol. 106, No. 10, 1999, pp. 889-909.

[21] Anderson, J. D., *Modern Compressible Flow with Historical Perspective*, Second Ed., McGraw-Hill, 1990.

[22] Jiang, G. S., and Shu, C. W., "Efficient Implementation of Weighted ENO Schemes," *Journal of Computational Physics*, Vol. 126, No. 1, 1996, pp. 202-228.

[23] Xu, S. J., Aslam, T., and Stewart, D. S., "High Resolution Numerical Simulation of Ideal and Non-Ideal Compressible Reacting Flows with Embedded Internal Boundaries," *Combustion Theory and Modelling*, Vol. 1, No. 1, 1997, pp. 113-142.

[24] Short, M., and Stewart, D. S., "Cellular Detonation Stability. Part 1. A Normal-Mode Linear Analysis," *Journal of Fluid Mechanics*, Vol. 368, 1998, pp. 229-262.

[25] Laney, C. B., *Computational Gasdynamics*, Cambridge University Press, Cambridge, 1998.

[26] LeVeque, R. J., *Finite Volume Methods for Hyperbolic Problems*, Cambridge University Press, Cambridge, 2002.

[27] Canuto, C., Hussaini, M. Y., Quarteroni, A., and Zang, T. A., *Spectral Methods in Fluid Dynamics*, Springer-Verlag, Berlin, 1988.

[28] Fornberg, B., *A Practical Guide to Pseudospectral Methods*, Cambridge University Press, Cambridge, 1996.

[29] Brooks, G. P., and Powers, J. M., "Standardized Pseudospectral Formulation of the Inviscid Supersonic Blunt Body Problem," *Journal of Computational Physics*, Vol. 197, No. 1, 2004, pp. 58-85.

[30] Henrick, A. K., Aslam, T. D., and Powers, J. M., "Highly Accurate Numerical Simulations of Pulsating One-Dimensional Detonations," AIAA Paper 2005-1173, Jan. 2005.

Independent Parameter	Units	Value
R	$J/kg/K$	287
α	$1/s$	1000
β	rad	$\pi/4$
γ	-	6/5
T_1	K	300
M_1	-	3
ρ_1	kg/m^3	1
q	J/kg	300000
Dependent Parameter	**Units**	**Value**
u_1	m/s	$18\sqrt{2870}$
p_1	Pa	86100
c_p	$J/kg/K$	1722
c_v	$J/kg/K$	1435

Table 1. Parameters used in sample oblique detonation calculations.

λ	X (m)	Y_w (m)	x (m)	y_w (m)	p (Pa)	T (K)	ρ (kg/m^3)
0.000000	0.000000	0.000000	0.000000	0.000000	86100.	300.000	1.00000
0.000000	0.000000	0.000000	0.000000	0.000000	414845.	423.416	3.41379
0.100000	0.021661	0.071842	0.066116	0.035483	406941.	439.454	3.22653
0.200000	0.047279	0.152154	0.141020	0.074158	398616.	455.334	3.05030
0.300000	0.078003	0.243204	0.227127	0.116815	389794.	471.027	2.88341
0.400000	0.115536	0.348314	0.327991	0.164599	380374.	486.496	2.72426
0.500000	0.162550	0.472633	0.449142	0.219261	370215.	501.688	2.57122
0.600000	0.223581	0.624787	0.599887	0.283695	359111.	516.525	2.42245
0.700000	0.307241	0.820947	0.797749	0.363245	346734.	530.883	2.27570
0.800000	0.433132	1.09742	1.08226	0.469723	332510.	544.549	2.12758
0.900000	0.664723	1.57005	1.58022	0.640165	315234.	557.069	1.97171
1.000000	∞	∞	∞	∞	291192.	567.048	1.78927

Table 2. Solution values along the wall streamline for flow parameters of Table 1.

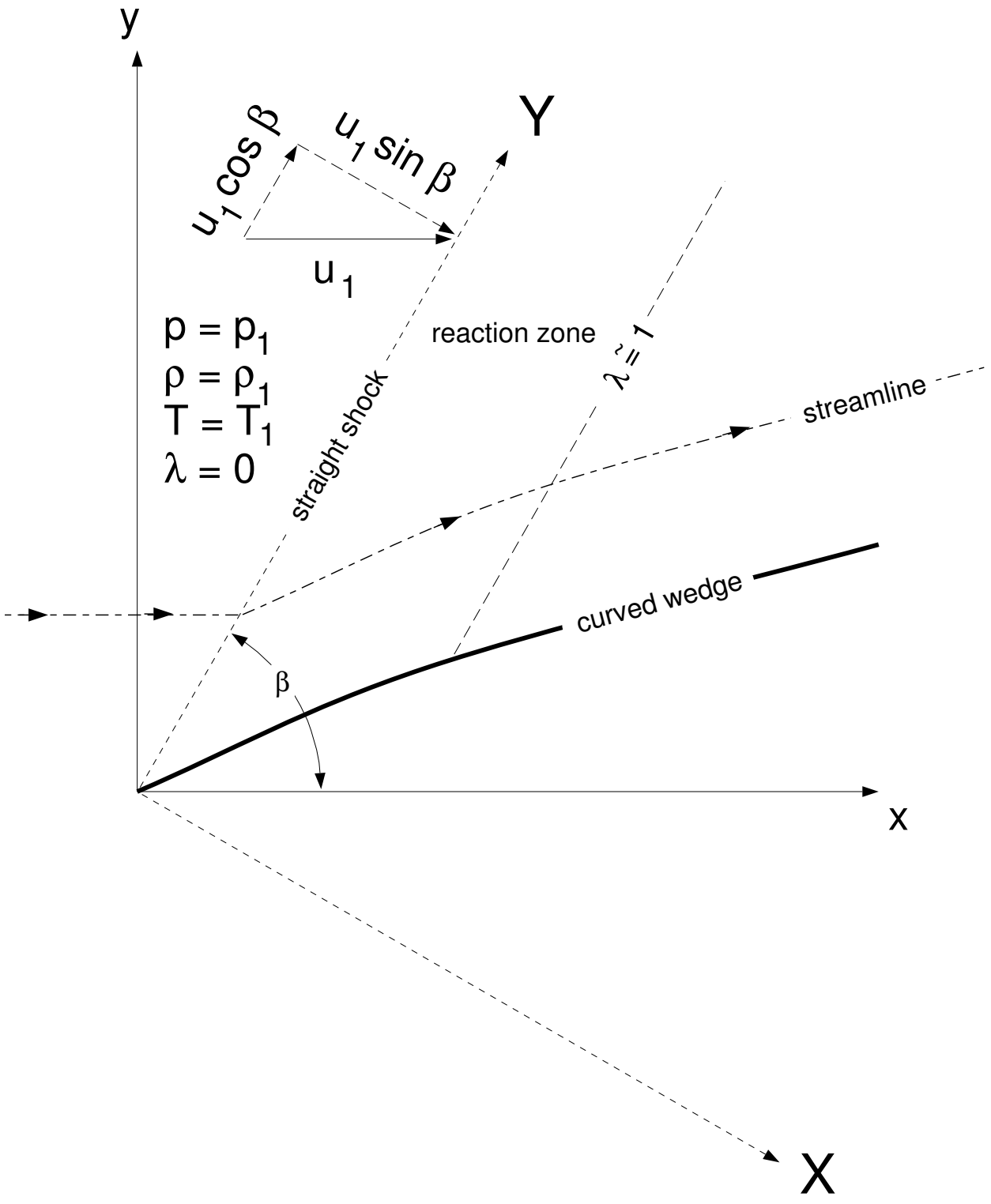

Figure 1. Schematic of configuration for straight-shock, curved wedge oblique detonation.

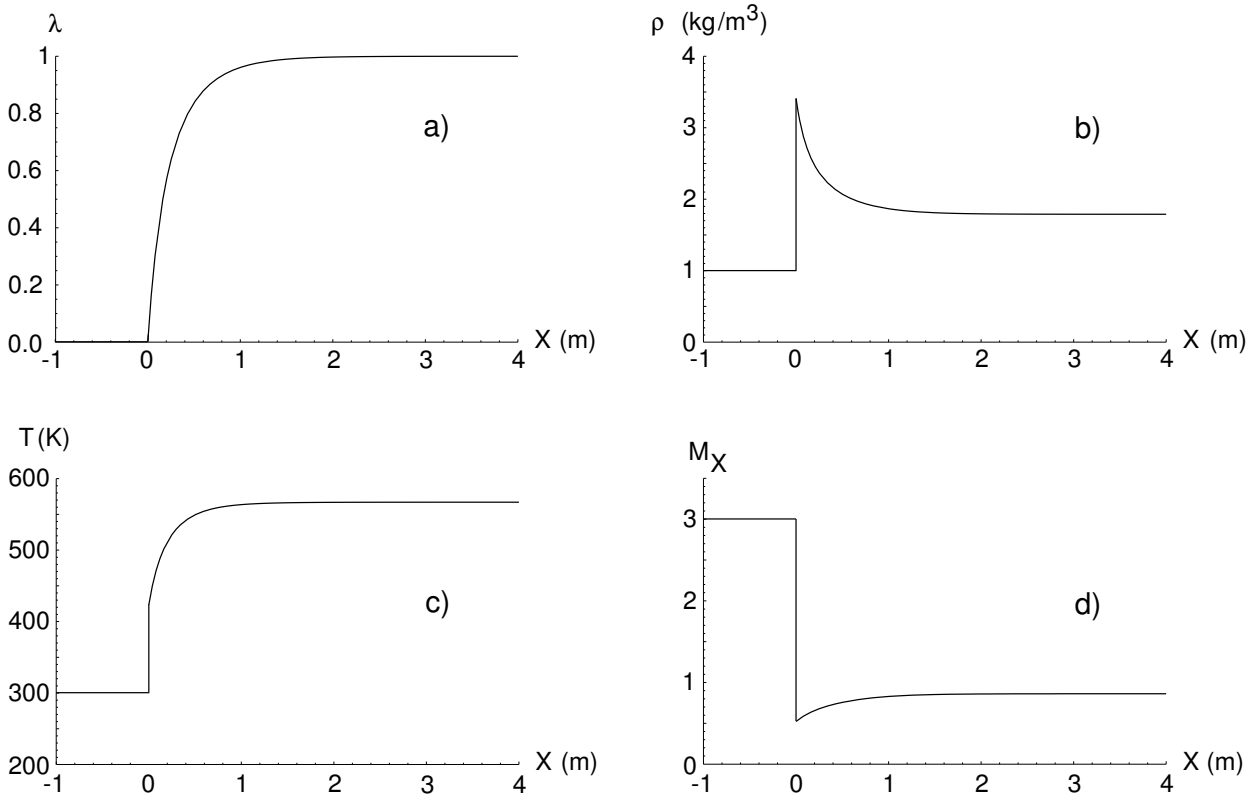

Figure 2. Exact solution for flow variables a) reaction progress, b) density, c) temperature, and d) Mach number normal to the shock, as function of normal distance from the shock, X, for parameters of Table 1.

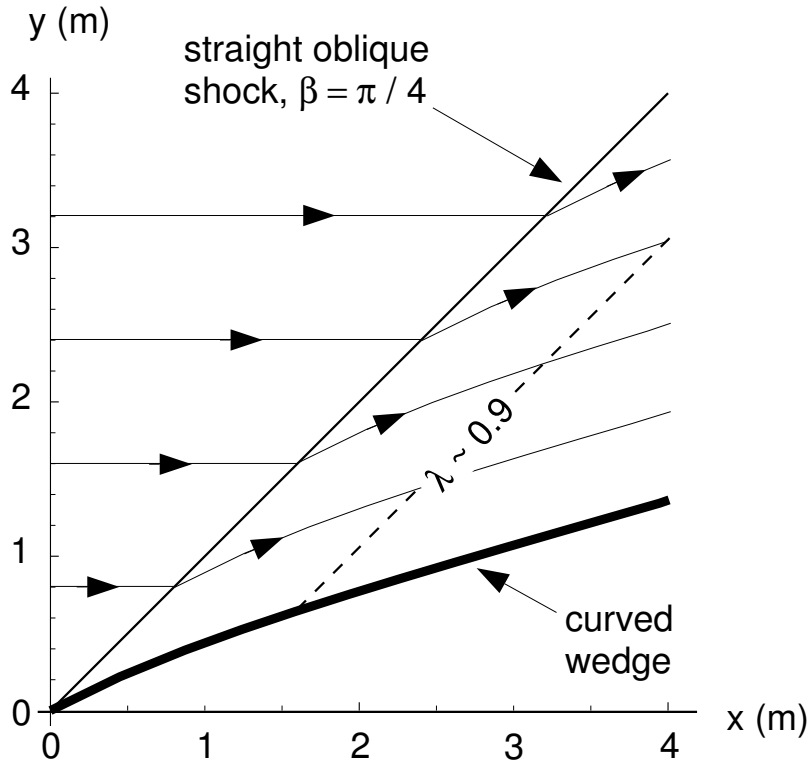

Figure 3. Exact solution for straight-shock, curved wedge oblique detonation streamlines for parameters of Table 1.

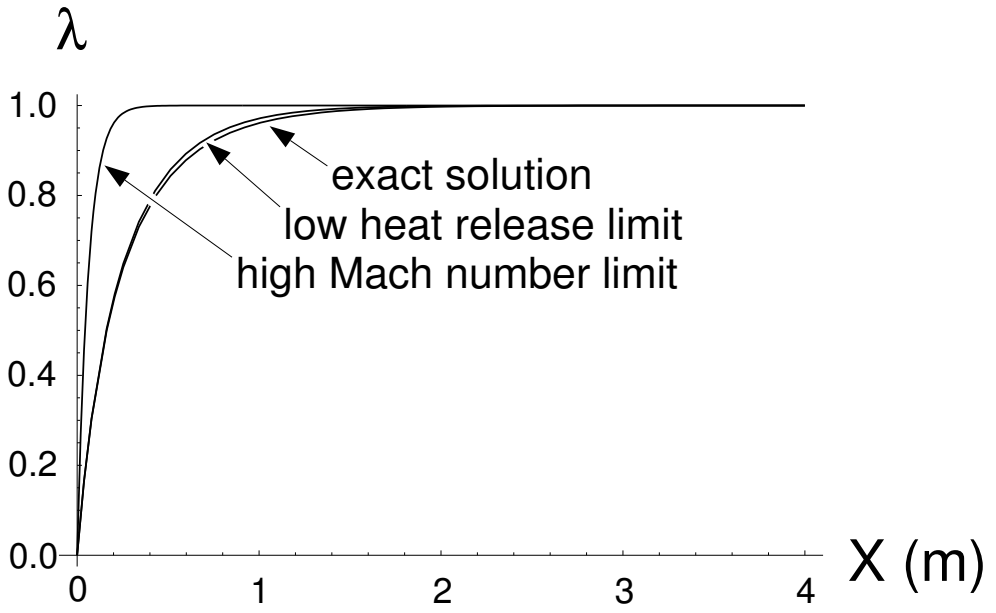

Figure 4. Predictions of reaction progress versus distance normal to the shock, X, from exact, low heat release limit, and high Mach number limit theories for parameters of Table 1.

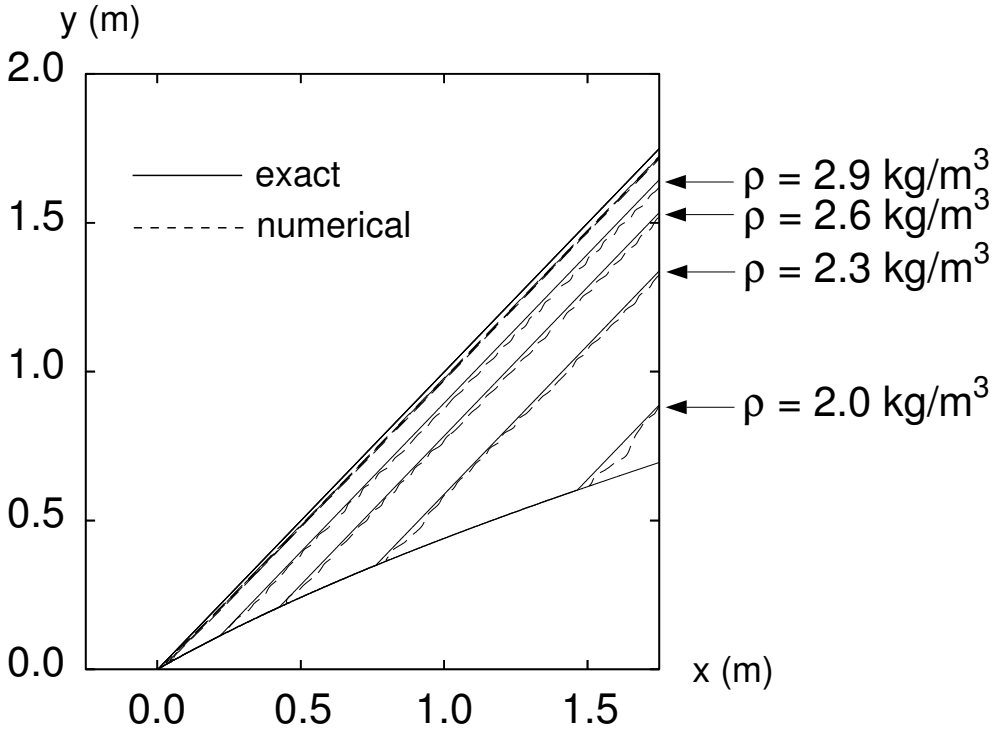

Figure 5. Predictions of shock locus and density contours from exact and numerical approximation for parameters of Table 1 and 256×256 grid.

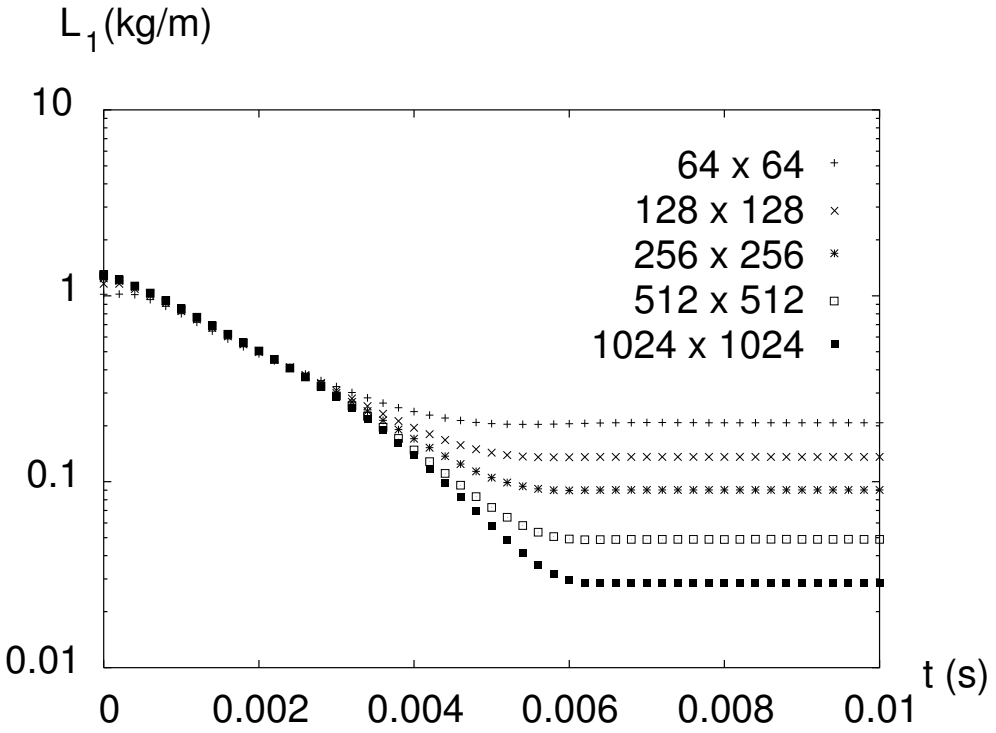

Figure 6. L_1 **residual norm for difference between predictions of density field from steady exact and time-dependent numerical methods as a function of time at several different grid resolutions for parameters of Table 1.**

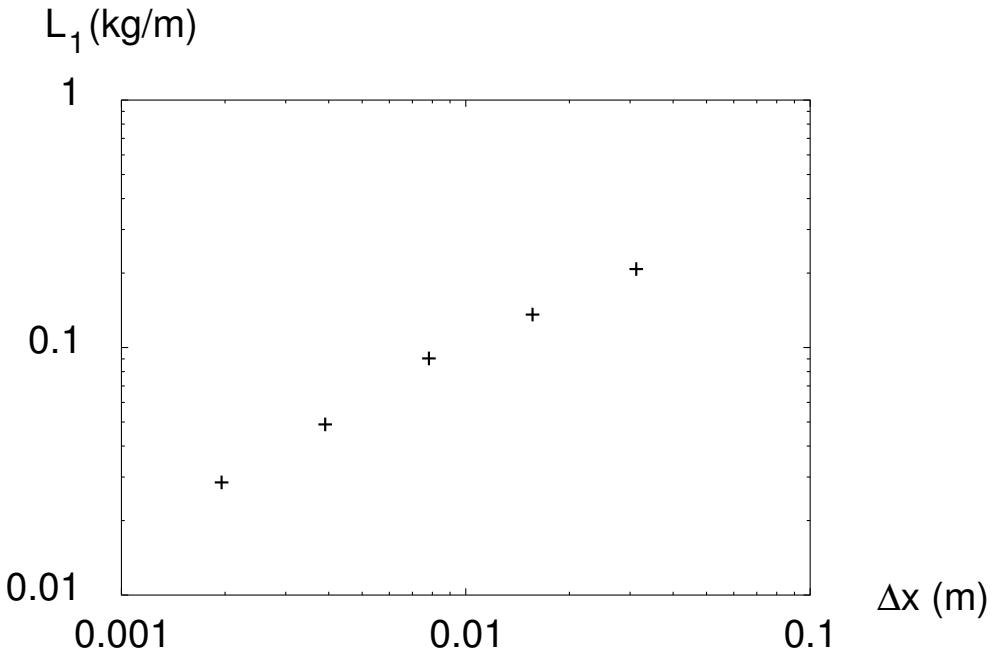

Figure 7. L_1 **error norm for difference between predictions of density field from exact and numerical methods in the long time limit as a function of grid size for parameters of Table 1; convergence rate** $\sim O(\Delta x^{0.779})$**.**